A EUROPEAN JOURNAL

CHEMPHYSCHEM

OF CHEMICAL PHYSICS AND PHYSICAL CHEMISTRY

Reprint

A Journal of ChemPubSoc Europe

WILEY-VCH

www.chemphyschem.org

ChemPubSoc Europe

DOI: 10.1002/cphc.201700788

CHEMPHYSCHEM Communications

Identifying the Crystalline Orientation of Black Phosphorus by Using Optothermal Raman Spectroscopy

Tianyu Wang[+],[a] Jing Liu[+],[a] Biao Xu,[b] Ridong Wang,[a] Pengyu Yuan,[a] Meng Han,[a] Shen Xu,[c] Yangsu Xie,[a] Yue Wu,[b] and Xinwei Wang*[a]

Current polarized Raman-based techniques for identifying the crystalline orientation of black phosphorus suffer significant uncertainty and unreliability because of the complex interference involving excitation laser wavelength, scattering light wavelength, and sample thickness. Herein, for the first time, we present a new method, optothermal Raman spectroscopy (OT-Raman), for identifying crystalline orientation. With a physical mechanism based on the anisotropic optical absorption of the polarized laser and the resulting heating, the OT-Raman can identify the crystalline orientation explicitly, regardless of excitation wavelength and sample thickness, by Raman frequency–power differential Φ ($=\partial\omega/\partial P$). The parameter Φ has the largest (smallest) value when the laser polarization is along the armchair (zigzag) direction. The OT-Raman technique is robust and is able to identify the crystalline orientation of BP samples with thicknesses up to 300 nm at a minimum and potentially as high as 1200 nm.

Black phosphorus (BP), a very new member of the two-dimensional materials family, has attracted worldwide attention due to its extraordinary electronic and optical properties, such as high carrier mobility and a thickness-dependent direct band gap.[1–7] As the most thermodynamically stable phosphorus allotrope, BP has a layered structure bonded together by van der Waals interactions. Inside an atomic single layer, each phosphorus atom is bonded covalently to three adjacent atoms to form a puckered honeycomb structure. Such asymmetric in-plane structure leads to an unique anisotropic nature in the optical,[1,6,8,9] electrical,[1,3,5,10] thermal[11–16] and mechanical[17–20] properties of BP. Normally, these anisotropic properties are characterized by two in-plane crystalline orientations, the armchair direction (AC) and zigzag direction (ZZ), respectively. The unique anisotropic properties of BP make it possible to develop novel electronic and optoelectronic devices. At the same time, however, the rapid and precise identification of the crystalline orientation of BP becomes of significant importance and urgency.

Although transmission electron microscopy (TEM) is the most straightforward technique to identify the crystalline orientation, its application is limited due to its relatively complicated and challenging sample preparation procedures, especially for BP.[8,15,21] Therefore, many new techniques have been developed, such as polarization-resolved infrared spectroscopy,[1] angle-resolved DC conductance,[1] and angle-resolved polarized Raman spectroscopy (ARPRS).[22] Among all these techniques, ARPRS is a widely used one due to its precise, simple and nondestructive features.[11,12] First reported by Wu et al., ARPRS has demonstrated that A_g^1, B_{2g} and A_g^2 peaks have periodical variation in Raman intensity as the rotation of BP sample under both parallel- and cross-polarization configurations.[22] This work concluded that the crystalline orientation of BP could be identified from the intensity variation of the A_g^2 mode under the parallel-polarization configuration, which has the smaller local maximum intensity in the zigzag direction and the larger local maximum intensity in the armchair direction. This conclusion was confirmed by Ribeiro et al., who conducted similar angular Raman experiments using 633, 532, and 488 nm lasers.[23] However, further research demonstrated that other factors, such as excitation wavelength and sample thickness, could also influence the polarization dependence of Raman intensity.[8,24] Ling et al. discovered that the armchair direction and zigzag direction could not be distinguished explicitly from the periodic variation of Raman intensity due to the influence of excitation wavelength and sample thickness.[8] Such influence, as suggested by Kim et al., results from the optical interference in the BP samples.[24] These works definitely manifest that ARPRS is not capable of distinguishing between the armchair direction and zigzag direction unambiguously unless the excitation wavelength and sample thickness are considered carefully.[8] However, these studies have paved a route for advancing the study of Raman spectroscopy as a novel and nondestructive method for determining the crystalline direction.

To overcome the drawbacks of ARPRS, but at same time take the advantage of Raman spectroscopy, a brand-new technique named optothermal Raman spectroscopy (OT-Raman) is developed in this work. The OT-Raman technique has a physical mechanism that can be traced back to the anisotropic optical absorption of BP samples. Compared to the ARPRS tech-

[a] T. Wang,[+] Dr. J. Liu,[+] R. Wang, P. Yuan, M. Han, Y. Xie, Prof. X. Wang
Department of Mechanical Engineering
Iowa State University
2025 Black Engineering Building, Ames, IA, 50010 (USA)
E-mail: xwang3@iastate.edu

[b] Dr. B. Xu, Prof. Y. Wu
Department of Chemical and Biological Engineering
Iowa State University
2114 Sweeney Hall, Ames, IA, 50010 (USA)

[c] Prof. S. Xu
Automotive Engineering College
Shanghai University of Engineering Science
333 Longteng Road, Shanghai (P. R. China)

[+] These authors contributed equally to this work

The ORCID identification number(s) for the author(s) of this article can be found under https://doi.org/10.1002/cphc.201700788.

nique which measures the periodic variation of Raman intensity, OT-Raman utilizes the Raman frequency–power differential Φ for crystalline orientation identification. The armchair and zigzag directions of BP samples can be easily identified and distinguished from the angular dependence of Φ to laser polarization. The maximization (minimization) of Φ in the armchair (zigzag) direction acts as the basic principle for identifying the crystalline orientation. Both experimental results and theoretical calculations have definitively proved the effectiveness of this principle regardless of the excitation wavelength and sample thickness. Hence, the OT-Raman technique is a new reliable tool to identify the crystalline orientation of BP samples precisely and nondestructively, which will benefit further development of BP-based electronic and optoelectronic devices.

BP samples are exfoliated from bulk BP crystal (99.998%, Smart Elements) using a modified mechanical exfoliation method.[25,26] In this method, the employment of viscoelastic stamp (PF-20/1.5-X4 Gelfilm from Gelpak) can reduce the polymer residues on the samples, and enable rapid identification of candidate BP sample with a specific thickness from its color contrast under normal illumination under an optical microscope. Then, the candidate BP sample on the surface of the viscoelastic stamp is transferred to a Si substrate and housed in an environment cell (Linkam Scientific) immediately. The whole air-exposure time of the BP sample is less than 2 min to avoid severe oxidation. The environment cell is filled with N_2 gas to avoid the degradation of BP samples in air.[25,27–29] A round fused silica window on the top lid of environment cell allows the irradiation of laser beam on the BP samples with negligible energy loss. By mounting the environment cell on a 3D microstage, the laser beam can be controlled to irradiate a specific spot of the BP samples precisely. The measurements are carried out using a BWTEK Voyage confocal Raman system at room temperature. All spectra are excited with a 532 nm laser (Excelsior-532-150-CDRH, Spectra-Physics) and collected in the backscattering configuration. We use a 20× objective to focus the excitation laser beam to a radius of 1.28 μm. Meanwhile, we use a half-wave plate to adjust the laser polarization. Moreover, a neutral density (ND) filter is applied to change the excitation laser power, which has transmittance of 16.5, 20.1, 25.0, 31.4, 41.9, 52.9, 62.1, 80.0 and 96.5%. Detailed system configurations can be found in our previous work.[30]

In the OT-Raman experiment, the laser polarization is changed with a 20° angle step until a total rotation of 360° is achieved. At each polarization angle, a series of laser powers from low to high are used to excite Raman scattering by adjusting output laser power using the ND filter. Raman frequency–power differential Φ can be extracted from the dependence of Raman frequency on the excitation laser power. Note that Φ is the most important indicator for identifying the crystalline orientation in the OT-Raman technique. It indeed reflects the temperature rise of the sample under unit power laser heating. After OT-Raman experiment, the thickness and morphology of BP samples are characterized by atomic force microscope (AFM). Importantly, transmission electron microscopy (TEM) is used to identify the crystalline orientation and confirm the results obtained by the OT-Raman technique.

The careful selection of appropriate BP crystallite for mechanical cleavage makes it possible for continuous exfoliation of thin BP samples from a single BP crystallite. We have found that thick and rectangular-shaped BP crystallite are perfectly suitable for continuous exfoliation. As a result, the crystalline orientation of one BP crystallite can be investigated by both OT-Raman technique and TEM. As the most straightforward technique for identifying crystalline orientation, TEM can confirm the validity of OT-Raman technique. The thin BP samples shown in Figure 1 and Figure 2 are indeed exfoliated from the same BP crystallite. They share exactly the same crystalline orientation considering their natural physical connection. Figure 1a and b show the TEM image and its corresponding electron diffraction pattern of a thin BP sample. They demonstrate that the [001] and [100] of the orthorhombic unit cell are along the armchair and zigzag directions, respectively. Meanwhile, the armchair (zigzag) direction is normal (parallel) to the naturally formed edge of BP sample.[24] Figure 2a shows the optical microscopy image of a thin BP sample labeled with crystalline orientation. In the Cartesian coordinates, the zigzag direction is along the *x* axis, and the armchair one is along the *y* axis. The zigzag direction angle is defined as 0°, which is also the initial angle of laser polarization. Four areas with uniform color contrast marked by the red stars are selected for the OT-Raman experiment. The height profile along the white lines in the AFM image (Figure 2b) shows the thicknesses of a, b, c and d areas. Their thicknesses are 24.6, 32.7, 90.1 and 97.7 nm (Figure 2c–f). The roughness of the BP surface results from the imperfect contact with the Si substrate, the slight oxidation of sample, as well as tiny amounts of gel material residues.

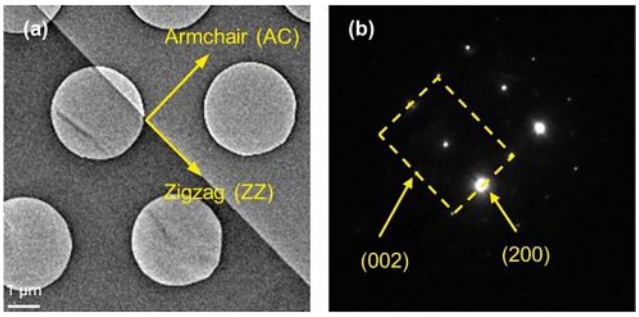

Figure 1. a) TEM image and b) the corresponding electron diffraction pattern of a thin BP sample. The armchair (zigzag) directions are normal (parallel) to the naturally formed crystalline edge.

Here, we take the 24.6 nm BP sample as an example to demonstrate the basic procedures and principles of the OT-Raman technique. To avoid laser heating damage on sample but excite a strong Raman signal at the same time, a careful selection of the appropriate output laser power is of great importance. For the 24.6 nm BP, an OT-Raman experiment is performed when the output laser power is 60 mW before attenuation by the ND filter. At each laser polarization angle, considering the natural energy loss of optical system and the attenuation of ND filter, the excitation laser powers irradiating on the BP surface are 7.69, 9.36, 11.65, 14.62, 19.54, 24.65, 28.94, 37.27

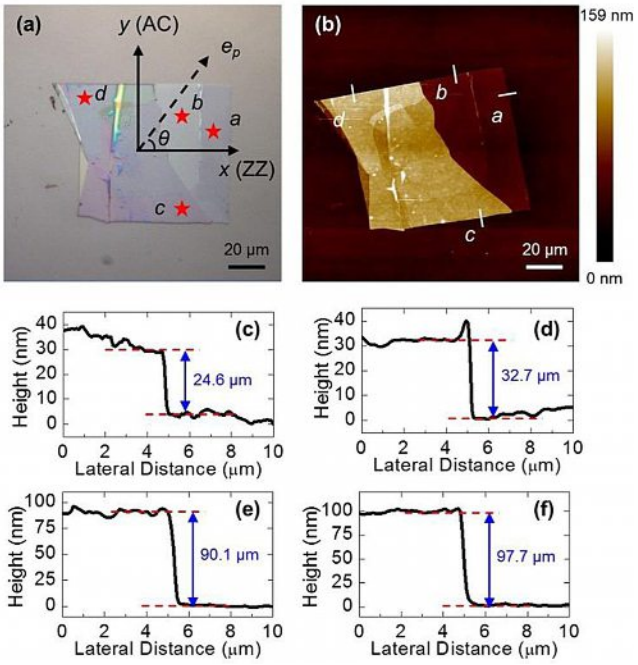

Figure 2. Top-left a) Optical microscope image of a thin BP sample deposited on a Si substrate. The zigzag (armchair) direction is along the *x* (*y*) axis of the Cartesian coordinates. e_p represents the laser polarization vector, θ denotes the angle between the *x* axis and laser polarization vector e_p. Four candidate areas (zones a, b, c, d) tested by OT-Raman experiment are marked by red stars. Top-right b) AFM image of the sample. Bottom-panels c–f) The height profile along the white lines in four areas (zones a, b, c and d as marked in the top-left and top-right panels (a) and (b)) are plotted to show their thicknesses. Their thicknesses are 24.6, 32.7, 90.1 and 97.7 nm.

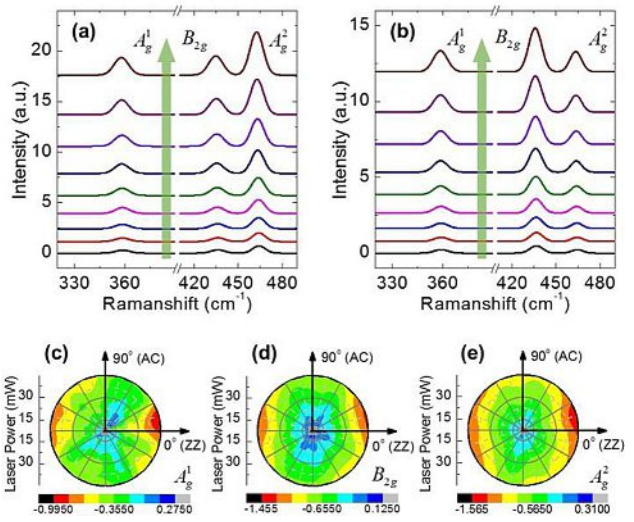

Figure 3. The Raman spectra of a 26.4 nm BP sample excited by different laser powers in the case of a) armchair-polarization and b) zigzag-polarization, respectively. These Raman spectra have been fitted by the Gaussian function. From the bottom spectrum to the top one, their corresponding excitation laser powers are 7.69, 9.36, 11.65, 14.62, 19.54, 24.65, 28.94, 37.27 and 44.92 mW, as shown by the green arrows. The contours of the angular variation of Raman shift against laser power are shown in c) A_g^1 d) B_{2g} and e) A_g^2.

and 44.92 mW. Figure 3a and b show Raman spectra excited by these laser powers when the laser polarization is along the armchair/zigzag direction. These Raman spectra have been fitted by the Gaussian function. Three Raman peaks A_g^1, B_{2g}, and A_g^2 are located at 359, 436 and 464 cm^{-1}. Obviously, in these two cases of laser polarization, the relative intensity of B_{2g} and A_g^2 modes change significantly, while that of A_g^1 remains almost unchanged. Most importantly, the increased excitation laser power leads to a red shift of the Raman frequency. Extensive studies have demonstrated that the A_g^1, B_{2g}, and A_g^2 Raman peaks are temperature-dependent, and the increased temperature leads to a decreased intensity (I), a red shift of Raman frequency (ω) and a broadening linewidth (Γ). Therefore, the frequency change of acquired Raman spectra allows one to monitor the local temperature change produced by the variation of the excitation laser power.

In the OT-Raman technique, the dependence of Raman frequency (ω) on the excitation laser power plays a vital role for determining the crystalline orientation. Figure 3c –e show the contours of the angular variation of A_g^1, B_{2g}, and A_g^2 Raman frequencies with excitation laser power. At each polarization angle, the Raman frequencies have been normalized by that excited by the lowest laser power. All the contours of Raman frequency show an elliptical pattern with an elongation along the armchair direction roughly, which indicates that BP has the largest temperature rise when the laser polarization is along the armchair direction. However, these Raman frequency contours, especially for the A_g^1one, show a large uncertainty which makes the determination of crystalline orientation difficult.

Instead of Raman frequency (ω), we have found that $\partial\omega/\partial P$ is a more useful and reliable parameter for determining crystalline orientation accurately with significantly reduced uncertainty. As we can see in Figure 4a, in both the cases of armchair polarization and zigzag polarization, the Raman frequency (ω) linearly depends on the excitation laser power as $\omega = \omega_0 + \Phi P$, where ω_0 is the Raman frequency at room temperature, and Φ, named as the Raman frequency–power differential, is the linear slope which represents the change in Raman frequency due to the irradiation of unit laser power. Φ of A_g^1, B_{2g}, and A_g^2 peaks are -0.0207 ± 0.0023, -0.0376 ± 0.0019 and -0.0413 ± 0.0010 cm^{-1}mW^{-1} in the armchair polarization, whereas they are -0.0113 ± 0.0018, -0.0217 ± 0.0015 and -0.0254 ± 0.0024 cm^{-1}mW^{-1} in the zigzag polarization. Obviously, the Φ value in the armchair-polarization is always larger than that in the zigzag polarization. The distinctively different Φ values in the armchair- and zigzag polarizations allows us to accurately determine the crystalline orientation. Figure 4b shows the Φ of A_g^1, B_{2g}, and A_g^2 peaks measured at each laser polarization angle, which share exactly the same polarization dependence. Apparently, they have the largest Φ value in the armchair direction and the smallest one in the zigzag direction. Φ has a periodic pattern of 180°, which can be fitted nicely by a $cos^2\theta$ function. The slight data dispersion can be attributed to several factors. They include the out-of-focus effect of the laser beam, the drift of laser spot along the BP surface and the non-uniform physical contact between BP and Si substrate. Since the Φ value of these three Raman peaks exhibit identical polarization dependence, any one of them can be used to identify

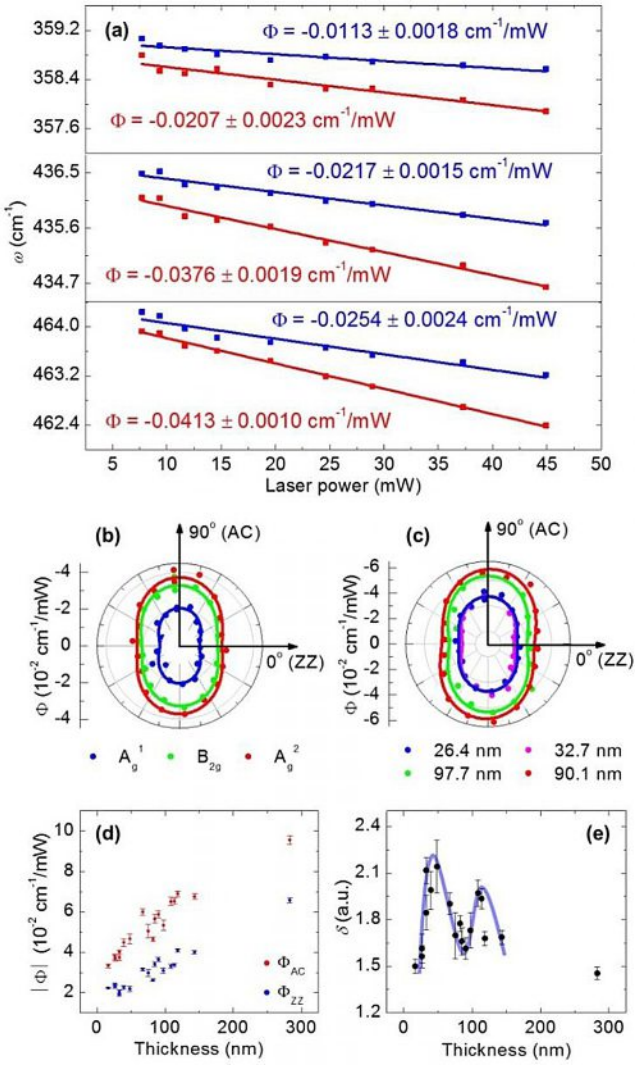

Figure 4. a) The dependence of A_g^1, B_{2g} and A_g^2 Raman frequency on the excitation laser power when the laser polarization is along the armchair direction (red) and zigzag direction (blue). The experimental data are fitted by a linear function. b) Polar plot of Φ for A_g^1 (blue), B_{2g} (green) and A_g^2 (red) modes. The dots are experimental data, and the lines are theoretical fitting curves. c) Polar plot of Φ for BP areas with thicknesses of 26.4 (blue), 32.7 (pink), 90.1 (red) and 97.7 nm (green). The dots are experimental data, and the lines are theoretical fitting curves. d) The variation of $|\Phi_{ac}|$ and $|\Phi_{zz}|$ as a function of BP thickness. Both $|\Phi_{ac}|$ and $|\Phi_{zz}|$ show a clearly increasing tendency. The error bars represent the standard error when experimental data are fitted by a $cos^2\theta$ function. e) The variation of δ values ($|\Phi_{ac}|/|\Phi_{zz}|$) as a function of BP thickness. The error bars represent the standard error. The blue line is used as a guide to the eye for the pattern of the δ-thickness variation.

the crystalline orientation. Here, we choose the A_g^2 peak since it has the largest Φ among all these three Raman peaks, as shown in Figure 4b. The large Φ of A_g^2 peak will reduce the data dispersion and improve the accuracy of crystalline orientation determination. In the following discussions, we will demonstrate that the polarization dependence of Φ results from the anisotropic optical absorption, and Φ is proportional to the optical absorbance.

To explore the BP-thickness influence on the polarization dependence of Φ, BP areas with thicknesses of 32.7, 90.1 and 97.7 nm (b, c, d, e) are also studied and their results are shown in Figure 4c. As we have expected, they have an exactly the same polarization dependence of Φ with the largest (smallest) value in the armchair (zigzag) polarization. Generally, thick BP samples tend to have a larger $|\Phi|$. In total, 19 BP samples with different thicknesses are mechanically exfoliated from three BP crystallites and tested. This thorough study proves the robustness of OT-Raman technique. The thinnest sample we have tested is 16.6 nm thick, and the thickest one is 282.7 nm thick. As presented in Figure 4d, $|\Phi|$ of both armchair and zigzag polarization ($|\Phi_{ac}|$ and $|\Phi_{zz}|$) increases with increased sample thickness, and $|\Phi_{ac}|$ is always larger than $|\Phi_{zz}|$. Defined as the ratio of $|\Phi_{ac}|$ to $|\Phi_{zz}|$, δ is used to quantitatively characterize the polarization dependence of Φ ($\delta = |\Phi_{ac}|/|\Phi_{zz}|$). The variation of δ against the sample thickness is plotted in Figure 4e. As shown by the blue guide line, the ratio δ oscillates with a damped amplitude with increased sample thickness. Note this oscillation is because of the interference of the excitation laser in the BP film. A detailed examination and discussions are given in theoretical studies (see below). Since all the measured samples have δ values much larger than 1, we can ascertain that Φ can be utilized for crystalline orientation identification at least for BP samples with a thickness up to 300 nm, and it has great potential to be applied to much thicker samples. Details will be discussed in the theoretical interpretation section.

The OT-Raman technique involves a complicated mechanism of optical absorption, heating, and thermal dissipation. When an incident laser beam irradiates the BP surface perpendicularly, both reflection and transmission happen at the air/BP interface. The transmitted part of laser beam will experience further alternate reflections at the BP/Si and BP/air interfaces. These multiple reflections in the BP layer can interfere destructively or constructively depending on the exact path length. The overall reflection from each interface is a sum of infinite number of reflections, and it can be described and calculated by the transfer matrix method (TMM). Figure 5a demonstrates the optical reflection and transmission in the BP–Si structure. I_0 is the optical intensity of incident laser beam, I_1 is the overall reflection intensity at the air/BP interface, I_2 is the overall reflection intensity at the BP/Si interface, and I_3 is the overall transmission intensity into Si substrate. Two key parameters in the TMM for calculating I_1 and I_2 are reflection index n and extinction coefficient k. Based on our literature reviews, the refractive indexes n is 3.02 in the armchair direction and 3.17 in the zigzag direction.[9] Calculated from the absorption coefficient α with expression $\alpha = 4\pi k/\lambda$, the extinction coefficients k is 0.216 and 0.135 in the armchair and zigzag directions.[8,31] Current literatures have reported a large variation in α values. Even in the same work, the calculated α cannot agree well with the measured one. However, all the work agrees that the absorption coefficient α in the armchair direction is larger than that in the zigzag direction. Our calculation of absorbance A based on n and k do have large uncertainty, but it nevertheless provides us basic idea of the evolution of A with the laser polarization and BP thickness, which is essential and sufficient to explain the physical mechanism of the OT-Raman technique.

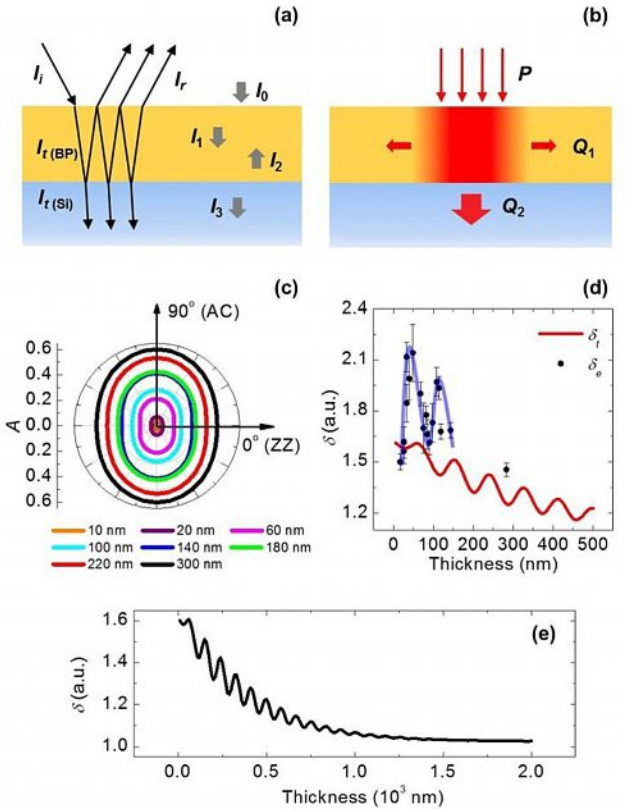

Figure 5. a) Optical transmission and reflection model of the incident laser beam in thin BP sample. To demonstrate the light transmission and reflection clearly, the incident light is deliberately plotted non-normal to the BP surface. b) Model of thermal transport for absorbed optical energy. Q_1 and Q_2 represent two approaches for dissipating thermal energy, in-plane thermal dissipation and across-interface thermal dissipation. c) Polar plot of the theoretical absorbance A for BP samples with different thicknesses. A has a maximum value in the armchair direction, and the minimum one in the zigzag direction. d) The variation of δ_e and δ_t values as a function of BP thickness. Experimental data δ_e are presented by black dots with error bars representing the standard deviation. The theoretical data δ_t are presented by a red line. The blue line is plotted to show the changing trend of δ_e. Both δ_e and δ_t exhibit an oscillating behavior with a decreased amplitude against increased thickness. e) The variation of δ_t in a thickness range up to 2000 nm.

First, we will demonstrate that Φ is proportional to A. Due to the anisotropic optical properties of BP, its volumetric optical absorption is expressed as $\dot{Q} = \dot{Q}_{ac} + \dot{Q}_{zz}$, where $\dot{Q}_{ac}$ and $\dot{Q}_{zz}$ are the volumetric optical absorption in the armchair direction and zigzag direction. $\dot{Q}_{ac}$ and $\dot{Q}_{zz}$ can be evaluated from the following equation [Eqs. (1) and (2)]:

$$\dot{Q}_{ac} = sin^2\theta\left[I_1 e^{-z/\tau_{ac}} + I_2 e^{-(h-z)/\tau_{ac}}\right]/\tau_{ac} \quad (1)$$

$$\dot{Q}_{zz} = cos^2\theta\left[I_1 e^{-z/\tau_{zz}} + I_2 e^{-(h-z)/\tau_{zz}}\right]/\tau_{zz} \quad (2)$$

where θ is the angle of laser polarization to the zigzag direction, h is the thickness of BP sample, τ_{ac} and τ_{zz} are the penetration depth in the armchair and zigzag directions ($\tau = 1/\alpha = \lambda/4\pi k$). Then, the total absorbance A in the BP sample can be written as [Eq. (3)]:

$$A = \int_0^h (\dot{Q}_{ac} + \dot{Q}_{zz})dz/I_0 \quad (3)$$

which leads to the expression [Eq. (4)]:

$$A = (I_1 + I_2)\cdot[1 - sin^2\theta\cdot exp(-h/\tau_{ac}) - cos^2\theta\cdot exp(-h/\tau_{zz})]/I_0 \quad (4)$$

Optical absorbance A is essential for unveiling the physical mechanism of the OT-Raman technique. Its relationship to $|\Phi|$ can be established from thermal transport model. In this model, the temperature distribution in the BP is obtained from the heat diffusion equation in the following form [Eq. (5)]:

$$k_{ac}\frac{\partial^2 T}{\partial x^2} + k_{zz}\frac{\partial^2 T}{\partial y^2} + k_{\perp}\frac{\partial^2 T}{\partial z^2} + \dot{Q}_{ac} + \dot{Q}_{zz} = 0 \quad (5)$$

where k_{ac} is the armchair thermal conductivity, k_{zz} is the zigzag thermal conductivity, and $k_{\perp}$ is the cross-plane thermal conductivity. The heat generated in BP sample due to the laser excitation is dissipated along the BP plane and across the BP/Si interface, as shown in Figure 5b. The steady temperature distribution is a result of competition between heat generation and thermal dissipation. Since mathematical solving of Equation (5) is impractical, the exact temperature distribution in the BP sample remains unknown. However, we can still conclude that T is proportional to $(\dot{Q}_{ac} + \dot{Q}_{zz})$ as Equation (5) is a linear differential equation. As a result, we have $\bar{T} \propto Q_{ac} + Q_{zz}$, where $\bar{T}$ is the average temperature rise of laser irradiating area detected by the Raman signal, and $Q_{ac} + Q_{zz}$ is the total laser absorption. Strictly speaking, such proportional relation works precisely for very thin BP sample (e.g. nm or tens of nm thickness), and deviates gradually as the thickness of BP sample increases. However, for our analysis of crystalline orientation, such proportional relationship is sufficient to identify the crystalline orientation. The normalization of $\bar{T} \propto Q_{ac} + Q_{zz}$ by the total incident laser power P leads to the expression $\partial\bar{T}/\partial P \propto A$, where A is the absorbance we have mentioned before. Combined with the well-known equation $\partial T/\partial P = \Phi\cdot\chi^{-1}$ in the Raman thermometry, we obtain the expression $\Phi \propto A\chi$, where χ is the temperature coefficient. χ defines the slope of the dependence of Raman frequency on the temperature, and it is a manifestation of the anharmonic terms in the lattice potential energy.[32] Considering the asymmetrical structure of BP, each P atom should also own an anisotropic potential which will further lead to a polarization-dependent χ. Previous work has reported the polarization-dependence of χ, which is $-0.02316\ cm^{-1}\ K^{-1}$ in the armchair direction and $-0.02700\ cm^{-1}\ K^{-1}$ in the zigzag direction for a 9.5-nm thick BP sample.[11] Note that the polarization dependence of χ is contradictory to that of A, and χ will weaken the final anisotropy of Φ contributed from A. Here, we simply regard χ as a constant due to their small difference in the armchair and zigzag directions. Then, the final expression relating Φ and A is $\Phi \propto A$. Figure 5c presents the dependence of calculated A on the laser polarization for BP samples with different thicknesses. Evidently, A has the maximum (minimum) value in the arm-

chair (zigzag) direction, and it increases with increased thickness. The polarization dependence presented by our calculated *A* is same with the one obtained by microabsorption measurement.[8] Therefore, the validity of Φ as the indicator for identifying crystalline orientation can be explained very well by the consistency of *A* dependence on the laser polarization.

Let us now discuss in detail about the parameter δ which characterizes the polarization dependence of Φ. As we mentioned above, the experimental δ (δ_e) value is defined as the ratio of $|\Phi_{ac}|$ to $|\Phi_{zz}|$. From the optical absorbance *A* and its proportional relationship to Φ, the theoretical δ (δ_t) can be defined as A_{ac}/A_{zz}. Compared with δ_e, δ_t provides us more information about the change of δ against thickness. As depicted in Figure 5d, δ_t decreases gradually and oscillates with a damped amplitude with increased sample thickness. In addition, when the BP thickness is thicker than 1200 nm, the oscillation of δ_t disappears and δ_t eventually is saturated at 1, as shown in Figure 5e. It indicates that the polarization dependence of *A* becomes weaker when the sample thickness becomes thicker, and there is a critical thickness from which the polarization dependence of *A* becomes negligible. The oscillation is due to the destructive or constructive effect during the multiple laser reflection within the BP sample. Although the amount of data δ_e is not relatively high enough, we can still generally recognize its decreasing trend with a damped oscillation when the sample thickness increases, which is similar to the change of δ_t. The period of oscillation is $\approx$74 nm uncovered by the experiment, which is close to that predicted by the theoretical calculation $\approx$85 nm. The smallest δ_e is $\approx$1.45 for a 282.7-nm BP sample, and the largest one is $\approx$2.14 for a 48.4-nm BP sample. Since δ_e is much larger than 1, we can guarantee that the OT-Raman technique is capable of identifying the crystalline orientation of BP samples with thickness up to 300 nm at least. Also, we notice that δ_e and δ_t cannot agree well with each other and δ_e is larger than δ_t in most cases. The discrepancy between δ_e and δ_t can be caused by inaccurate measurement of *n* and *k* reported in literatures, the neglected anisotropic effect of χ, as well as the approximations used for the proportional relationship between Φ and *A*. Because it is out of the scope of this work, the influence of these factors on such discrepancy is not discussed. Nevertheless, we conclude that the OT-Raman technique has a very strong capability for identifying the crystalline orientation of BP samples as thick as 300 nm. The theoretical calculation further suggests that the thickness limitation for using OT-Raman can be as large as 1200 nm. No matter what the real thickness limitation is, the capability of OT-Raman technique is remarkable enough in typical research which the studied BP samples are normally thinner than 100 nm.

We have developed the OT-Raman technique for identifying the crystalline orientation of BP. In this technique, the Raman frequency–power differential Φ (reflecting the temperature rise of the sample) is utilized as an indicator, which has the largest value in the armchair direction and the smallest one in the zigzag direction, regardless of excitation wavelength and sample thickness. The OT-Raman technique is robust: It is independent of the excitation laser wavelength, the scattering Raman wavelength, and the sample thickness. The OT-Raman technique is able to identify the crystalline orientation of BP samples with thickness of up to 300 nm at least. The thickness limit for applying the OT-Raman technique is still unclear, but the theoretical calculation has suggested that it can be as large as 1200 nm. Considering the thin thickness of BP samples normally studied, the capacity of the OT-Raman technique is strong enough to characterize their crystalline orientation explicitly. This technique has great potential to be applied to other anisotropic materials, which will pave a route for significantly advancing the study of anisotropic properties of materials.

Acknowledgements

Support of this work by National Science Foundation (CBET1235852, CMMI1264399) and Department of Energy (DENE0000671, DEEE0007686) is gratefully acknowledged.

Conflict of interest

The authors declare no conflict of interest.

Keywords: black phosphorus · crystalline orientation · nanostructures · polarization dependence · Raman spectroscopy

[1] F. N. Xia, H. Wang, Y. C. Jia, *Nat. Commun.* **2014**, *5*, 4458.
[2] L. K. Li, Y. J. Yu, G. J. Ye, Q. Q. Ge, X. D. Ou, H. Wu, D. L. Feng, X. H. Chen, Y. B. Zhang, *Nat. Nanotechnol.* **2014**, *9*, 372–377.
[3] H. Liu, A. T. Neal, Z. Zhu, Z. Luo, X. F. Xu, D. Tomanek, P. D. D. Ye, *ACS Nano* **2014**, *8*, 4033–4041.
[4] M. Buscema, D. J. Groenendijk, S. I. Blanter, G. A. Steele, H. S. J. van der Zant, A. Castellanos-Gomez, *Nano Lett.* **2014**, *14*, 3347–3352.
[5] J. S. Qiao, X. H. Kong, Z. X. Hu, F. Yang, W. Ji, *Nat. Commun.* **2014**, *5*, 4475.
[6] X. M. Wang, A. M. Jones, K. L. Seyler, V. Tran, Y. C. Jia, H. Zhao, H. Wang, L. Yang, X. D. Xu, F. N. Xia, *Nat. Nanotechnol.* **2015**, *10*, 517–521.
[7] V. Tran, R. Soklaski, Y. F. Liang, L. Yang, *Phys. Rev. B* **2014**, *89*, 235319.
[8] X. Ling, S. X. Huang, E. H. Hasdeo, L. B. Liang, W. M. Parkin, Y. Tatsumi, A. R. T. Nugraha, A. A. Puretzky, P. M. Das, B. G. Sumpter, D. B. Geohegan, J. Kong, R. Saito, M. Drndic, V. Meunier, M. S. Dresselhaus, *Nano Lett.* **2016**, *16*, 2260–2267.
[9] N. N. Mao, J. Y. Tang, L. M. Xie, J. X. Wu, B. W. Han, J. J. Lin, S. B. Deng, W. Ji, H. Xu, K. H. Liu, L. M. Tong, J. Zhang, *J. Am. Chem. Soc.* **2016**, *138*, 300–305.
[10] R. X. Fei, L. Yang, *Nano Lett.* **2014**, *14*, 2884–2889.
[11] Z. Luo, J. Maassen, Y. X. Deng, Y. C. Du, R. P. Garrelts, M. S. Lundstrom, P. D. Ye, X. F. Xu, *Nat. Commun.* **2015**, *6*, 8572.
[12] H. J. Jang, J. D. Wood, C. R. Ryder, M. C. Hersam, D. G. Cahill, *Adv. Mater.* **2015**, *27*, 8017–8022.
[13] Y. Wang, G. Z. Xu, Z. P. Hou, B. C. Yang, X. M. Zhang, E. K. Liu, X. K. Xi, Z. Y. Liu, Z. M. Zeng, W. H. Wang, G. H. Wu, *Appl. Phys. Lett.* **2016**, *108*, 092102.
[14] B. Sun, X. Gu, Q. Zeng, X. Huang, Y. Yan, Z. Liu, R. Yang, Y. K. Koh, *Adv. Mater.* **2017**, *29*, 1603297.
[15] S. Lee, F. Yang, J. Suh, S. J. Yang, Y. Lee, G. Li, H. S. Choe, A. Suslu, Y. B. Chen, C. Ko, J. Park, K. Liu, J. B. Li, K. Hippalgaonkar, J. J. Urban, S. Tongay, J. Q. Wu, *Nat. Commun.* **2015**, *6*, 8573.
[16] T. Wang, R. Wang, P. Yuan, S. Xu, J. Liu, X. Wang, *Adv. Mater. Interfaces* **2017**, 1700233.

[17] H. Chen, P. Huang, D. Guo, G. X. Xie, *J. Phys. Chem. C* **2016**, *120*, 29491 – 29497.
[18] H. Y. Sun, G. Liu, Q. F. Li, X. G. Wan, *Phys. Lett. A* **2016**, *380*, 2098 – 2104.
[19] J. W. Jiang, H. S. Park, *J. Phys. D* **2014**, *47*, 385304.
[20] Q. Wei, X. H. Peng, *Appl. Phys. Lett.* **2014**, *104*, 251915.
[21] X. L. Liu, J. D. Wood, K. S. Chen, E. Cho, M. C. Hersam, *J. Phys. Chem. Lett.* **2015**, *6*, 773 – 778.
[22] J. X. Wu, N. N. Mao, L. M. Xie, H. Xu, J. Zhang, *Angew. Chem. Int. Ed.* **2015**, *54*, 2366 – 2369; *Angew. Chem.* **2015**, *127*, 2396 – 2399.
[23] H. B. Ribeiro, M. A. Pimenta, C. J. S. de Matos, R. L. Moreira, A. S. Rodin, J. D. Zapata, E. A. T. de Souza, A. H. C. Neto, *ACS Nano* **2015**, *9*, 4270 – 4276.
[24] J. Kim, J. U. Lee, J. Lee, H. J. Park, Z. Lee, C. Lee, H. Cheong, *Nanoscale* **2015**, *7*, 18708 – 18715.
[25] A. Castellanos-Gomez, L. Vicarelli, E. Prada, J. O. Island, K. Narasimha-Acharya, S. I. Blanter, D. J. Groenendijk, M. Buscema, G. A. Steele, J. Alvarez, *2D Mater.* **2014**, *1*, 025001.
[26] A. Castellanos-Gomez, M. Buscema, R. Molenaar, V. Singh, L. Janssen, H. S. J. van der Zant, G. A. Steele, *2D Mater.* **2014**, *1*, 011002.
[27] J. O. Island, G. A. Steele, H. S. J. van der Zant, A. Castellanos-Gomez, *2D Mater.* **2015**, *2*, 011002.
[28] A. Favron, E. Gaufres, F. Fossard, A. L. Phaneuf-L'Heureux, N. Y. W. Tang, P. L. Levesque, A. Loiseau, R. Leonelli, S. Francoeur, R. Martel, *Nat. Mater.* **2015**, *14*, 826 – 832.
[29] J. D. Wood, S. A. Wells, D. Jariwala, K. S. Chen, E. Cho, V. K. Sangwan, X. L. Liu, L. J. Lauhon, T. J. Marks, M. C. Hersam, *Nano Lett.* **2014**, *14*, 6964 – 6970.
[30] P. Yuan, C. Li, S. Xu, J. Liu, X. Wang, *Acta Mater.* **2017**, *122*, 152 – 165.
[31] J. G. Weaver, H. P. R. Frederikse, *CRC Handbook of Chemistry and Physics, 87 ed.* (Eds.: D. R. Lide), Taylor & Francis, Abingdon-on-Thames, **2007**, pp. 116 – 140.
[32] I. Calizo, A. A. Balandin, W. Bao, F. Miao, C. N. Lau, *Nano Lett.* **2007**, *7*, 2645 – 2649.

Manuscript received: July 17, 2017
Accepted manuscript online: August 16, 2017
Version of record online: August 25, 2017